Haiqin Zhu[1*], Debin Kong[2], Fulai Xiao[3], Hengxin Lei[4]

Ice-Core Micro-CT Image Segmentation with Dual Stream Spectrum Deconvolution Neural Network and Gaussian Mixture Model

JES Journal of Electrical Systems

Abstract: - Polar ice sheets, or ice cores, are among the most well-known natural archives that might provide crucial historical details about our planet's previous environment. An important factor in establishing the fundamental characteristics of ice, likes pore close-off, albedo, melt events, is the ice-core microstructure. To engulf these complications Ice-Core Micro-CT Image Segmentation with Dual Stream Spectrum Deconvolution Neural Network and Gaussian Mixture Model (ICMCTS-WSOA-DSSDNN-GMM)is proposed. Initially, micro scale CT images are collect from Alfred Wegener Institute ice-core storage as input. Then,data's are given to pre-processing. In pre-processing, it enhance image brightness, remove salt pepper noise, crop outer ring (carbon fiber casing) to have only ice particles in image utilizing Federated Neural Collaborative Filtering (FNCF).The pre-processing output is given to segmentation. Here, micro scale CT image is utilized for segmenting high-resolution scans using Gaussian Mixture Model (GMM). After that, the segmented images are given to Dual Stream Spectrum Deconvolution Neural Network optimized with Water Strider Optimization Algorithm for classifying micro scale CT images as sintered snow, compacted firn and bubbly ice. The proposed ICMCTS-WSOA-DSSDNN-GMM method is executed in python. The performance of ICMCTS-WSOA-DSSDNN-GMM approach attains 16.24%, 17.90% and 27.7% high accuracy, 14.04%, 25.51% and 19.31% higher precision and 14.36%, 12.65%, 14.51% higher recall analyzed with existing techniques likes Ice-Core Micro-CT Image Segmentation With Deep Learning and Gaussian Mixture Method (ICMCTS-U-net-GMM), Computer Aided Detection of COVID 19 from CT Images Depend on Gaussian Mixture Method with Kernel Support Vector Machines Classifer (ICMCTS-KNN-GMM) and the Gmmseg: Gaussian mixture based generative semantic segmentation methods(ICMCTS-FCN-GMM) respectively.

Keywords: Alfred Wegener Institute ice-core storage, Federated Neural Collaborative Filtering, micro scale CT image, Gaussian Mixture Model (GMM), Dual Stream Spectrum Deconvolution Neural Network, Water Strider Optimization Algorithm (WSOA).

I. INTRODUCTION

Over time, snow builds up in the polar ice sheets of Greenland, Antarctica, where weight of snow layers above causes the snow to consolidate [1]. The snow grains become more closely packed as a outcome of this compaction, creating a more dense structure that includes firn, ice, and sintered snow [2, 3]. The firn beneath the snow gets denser with time and has the potential to solidify into glacial ice [4]. It may take several years or perhaps centuries for this change to occur based on variables including weather, temperature, and precipitation, among others [5, 6]. Air bubbles encased in ice are the remnants of air that was formerly part of open pore structure of snow [7]. Such air bubbles are momentary representations of previous atmosphere [8].Because they can retain a variety of proxies over timescales ranging from decades to hundreds millennia, such as greenhouse gas concentrations and aerosol-linked atmospheric impurity records, polar ice cores are excellent source of historical climate data [9, 10]. They can also be used as tool to track history of global temperature [11]. Microstructure is main ice core's primary characteristics. Ice-core microstructure holds priceless information on optical characteristics, melting events, global warming [12, 13].The transition from snow to ice usually happens in the upper 120 metres [14]. Therefore, research into this depth range is required to comprehend the driving processes. Both ice-core dating and the determination of pore close-off point the age difference among ice, gas rely heavily on structure of snow/firn column [15]. This investigation will concentrate on this particular region of the ice core. CT imaging is most promising techniques for analysing ice-core microstructure. CT scan data consists of series of 2D images that are horizontal slices of core; each 2-D image is taken into consideration separately in this investigation [16]. There are several types, modalities, resolutions, and ice properties available for capturing ice-core micro-CT images [17]. Hence, CT pictures of a porous substance (such as an ice-air mixture) with varying densities are produced along top 120 m of the ice core, beginning by lower-density snow (0.08 g/cm3), followed by middle-density firn (0.35 g/cm3), higher-density polar ice (0.91 g/cm3).

[1]Associate professor, Scientific Research Office, Yantai Nanshan University, Yantai, Shandong, 265713, China
[2]Professor, Scientific Research Office, Yantai Nanshan University, Yantai, Shandong, 265713, China
[3]Engineer,Technology Center, Shandong Nanshan Science and Technology Research Institute, Yantai, Shandong, 265713, China
[4]Lecturer, School of Economics and Management, Yantai Nanshan University, Yantai, Shandong, 265713, China
*Corresponding author e-mail: ytnszhq@126.com

Creating a reliable picture segmentation tool for wide variety of densities is a significant task [18].The two primary categories of state-of-the-art processes utilized for image segmentation as follows [19]. Traditional algorithmic-depend methods, including region-growing active contour, random walk, graph-cut methods, comprise the first group. These models are capable of numerous computations during the segmented mask production process, and some of them are susceptible to variations in the picture histogram and intensity value range [20]. Additionally, they need human input from the user in order to achieve an appropriate segmentation. For instance, the user must supply the parameters for graph formation, adjacency matrices, energy functions, seeds for region growth, and so forth.

The requirement for operator interference in each metre of ice is a drawback of this technology. Moreover, the Z-direction noise (noise propagating between layers). Global thresholding isn't practical method for segmenting ice-core CT images because ice density, image noises vary across dataset, making it impossible to use a single threshold for entire specimen without increasing segmentation uncertainty [21]. Furthermore, it is impractical to supply manual thresholds for every image in collection. In addition, there is a significant range of scattering that varies by varying ice densities because of crystal structure of the ice particles. Existing technique doesn't attains sufficient accuracy, computational time is increases that are motivated us to do this investigation work.

Major contributions of proposed method are abridged below,

- In this research, Ice-Core Micro-CT Image Segmentation with Dual Stream Spectrum Deconvolution Neural Network and Gaussian Mixture Model (ICMCTS-WSOA-DSSDNN-GMM) is proposed.
- Micro scale CT images are collect from Alfred Wegener Institute ice-core storage. Develop a Federated Neural Collaborative Filtering (FNCF) it improve image brightness, remove salt pepper noise, crop outer ring to have only ice particles in image.
- Propose a WSOA to optimize DSSDNN.
- The efficacy of proposed model is analysed with the existing techniques likes ICMCTS-U-net-GMM, ICMCTS-KNN-GMM and ICMCTS-FCN-GMM respectively.

Rest of these manuscripts is organized as follows: Part 2 reviews literature review, Part 3 designates proposed method, Part 4 shows results, Part 5 conclusion.

II. LITERATURE REVIEW

Numerous investigation studies were presented in the literature linked to deep learning depend ICMCTS, some current works are reviewed here,

Bagherzadeh, et al. [22] have suggested ICMCTS with DL and GMM. Here, presents new method to enhance segmentation of porous microstructures: DL method (U-net) was trained on higher-resolution (30 μm) data using weak segmentation [GMM] as ground truth, in order to segment low-resolution (60 μm) data. With intersection over the union and an F1-score, this methodology has achieved excellent segmentation accuracy in quantitative measures, showing a significant improvement over thresholding, unsupervised techniques. Additionally, U-net segmentation outcomes were more accurate in capturing the specimen's true weight, density, specific surface area. It provides high precision and low Jaccard index.

Saygılı et al. [23] have presented computer-assisted detection of COVID-19 from CT images depend on GMM with kernel support vector machines classifier. Here, three fundamental steps make up the study: segmentation, classification, and preprocessing. The preprocessing stage of image processing includes image resizing, image sharpening, noise reduction, contrast stretching. The segmentation stage utilizes a Gaussian Mixture Model based on expectation–maximization. Using kernel support vector machines approach in conjunction with kNN, decision trees, two distinct ensemble techniques, COVID-19 was classified as positive, negative during the classification step. It provides high recall and low F1-score.

Liang et al. [24] have suggested that the Gmmseg: Gaussian mixture depend generative semantic segmentation methods. Here, a new family of segmentation models called GMMSeg was put out by us. It was based on dense generative classifier for joint distribution p (pixel feature andclass). In order to capture class-conditional densities, GMMSeg uses Expectation-Maximization (EM) to construct Gaussian Mixture Models (GMMs) for each class. Concurrently, deep dense representation undergoes E2E discriminative training, whereby it maximises p(class pixel feature). It attains higher computational time, lower error rate.

Wang et al. [25] have presented crowd localization from gaussian mixture scoped knowledge with scoped teacher. Here, to address scale distribution confusion caused by intrinsic scale shift, paper focuses on access. To

regularise chaotic scale distribution, we suggest using Gaussian Mixture Scope. To address measure distribution, the GMS, in practice, decouples the mixture method into sub-normal distributions and applies a Gaussian mixed distribution to regularise the chaos inside the sub-distributions. Next, in order to normalise the disarray among sub-distributions, an alignment is implemented. Even yet, overfitting results from GMS's ability to push hard samples in training set aside, despite the fact that it was effective in regularising data distribution. It provides high recall and low precision.

Goel et al. [26] have presented Probabilistic Point Cloud Modelling via Self-Organizing GMM. Here, offers finite Gaussian Mixture Model (GMM) continuous probabilistic modelling method for spatial point cloud data, where components was adjusted allowing to scene complexity. There aren't many hierarchical or adaptive solutions available to deal with the problem of striking balance among method fidelity, size. Rather, cutting-edge mapping techniques don't generalise across different contexts; instead, they need to have parameters adjusted for particular use cases. It attains higher accuracy, lower recall.

Ajay et al. [27] have presented that the unsupervised hyper spectral microscopic image segmentation utilizing deep embedded clustering process. In this paper, though they can solve puzzles, AI systems were still restricted. When machine learning is ineffective, deep learning is employed. A lot of data is required for supervised learning. In modern AI, deep learning was essential. A sizable labelled dataset is necessary for supervised learning. The choice of criteria keeps things from fitting too or too little. The above-mentioned difficulties are solved through unsupervised learning (carried out by the clustering method). Two processing steps were taken to achieve this: transforming data into a latent feature space using nonlinear deep learning networks. It provides high Jaccard index and low precision.

Xiong, et al. [28] have presented identification of cash crop diseases utilizing automatic image segmentation process with DL expanded dataset. Here, offer a deep learning approach with an enlarged dataset that uses automatic image segmentation to identify illnesses in cash crops. Goal of the Automatic Image Segmentation Algorithm, which was depend on GrabCut process, was to automatically extract disease spots from images though preserving background information. When processing images, it eliminates the requirement for human object selection and takes a lot less time than the GrabCut algorithm. In order to increase Mobile Net's capacity for generalisation, the public dataset Plant Village is expanded with large number of crop photos from Internet, useful planting bases. It attains higher F1-score, lower computational time.

III. PROPOSED METHODOLOGY

The ICMCTS-WSOA-DSSDNN-GMM is discussed. This section presents clear depiction about research method utilized in Ice-Core Micro-CT Image Segmentation from micro scale CT images. The block diagram of ICMCTS-WSOA-DSSDNN-GMM is signified by Figure 1. Thus, detailed explanation about ICMCTS-WSOA-DSSDNN-GMM is given below

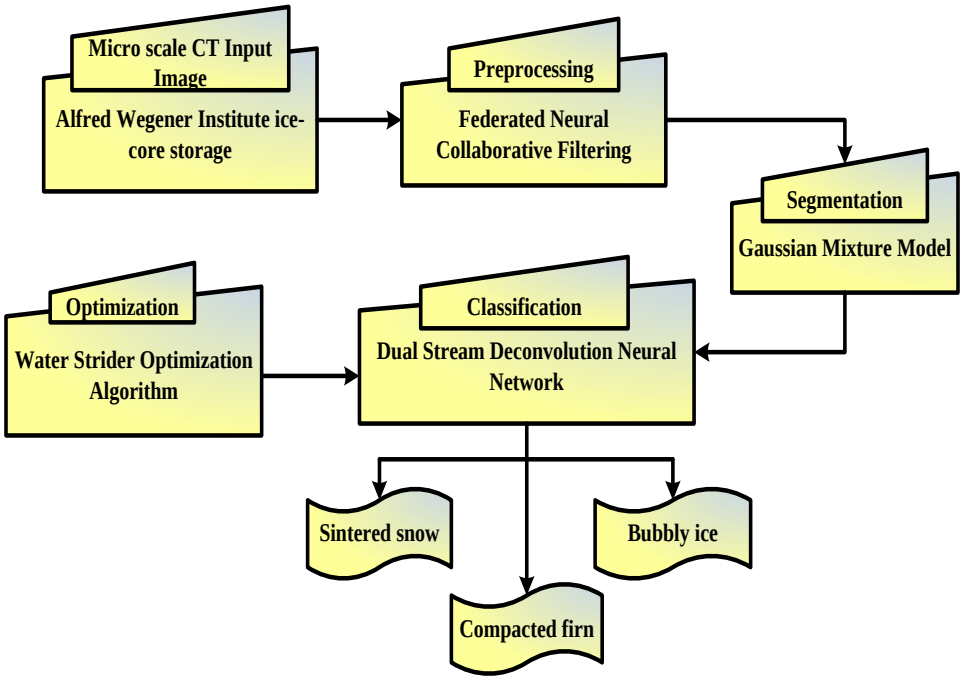

Figure 1: Block diagram of ICMCTS-WSOA-DSSDNN-GMMIce-Core Micro-CT Image Segmentation

A. Image Acquisition

Initially, micro scale CT images are collect from Alfred Wegener Institute ice-core storage as input. Three ice cores (specimens) were moved to AWI-Ice-CT lab while taking into account frozen transport protocols (<-20 ◦C) from Alfred Wegener Institute's ice-core storage. The lab's CT scan machine create micro measure CT scans from ice cores that are no longer than one metre and no wider than fifteen centimetres, and the X-ray machine source creates cone-shaped beams.

B. Pre-processing utilizing Federated Neural Collaborative Filtering

In this step, data pre-processing using FNCF [29] is discussed. FNCF it improve image brightness, remove salt pepper noise, crop outer ring to have only ice particles in image. Federated neural Collaborative Filtering method makes it feasible to train models without revealing local data, sending raw client updates presents further privacy concerns. In order to solve this specific problem, researchers employ a secure collection technique that satisfies safety requirements for an honest but inquiring organization. To calculating the standard predictive distribution is given in equation (1),

$$W_{v+1} \leftarrow \sum_{i=1}^{|c|} \frac{m_i}{m} W_{v+1}^{i} \tag{1}$$

Where, $|c|$ represents number of input data, m_i denotes number of reduces the data, $\sum_{i-1}^{|c|}$ signifies total redundancy of data and W_{v+1}^{i} relevant information produced by the involved entity i . To remove the duplicates of the data is given in equation (2),

$$WI_{v+1}^{i} + I_{v+1}^{i} + \sum_{i \in c: i<j} IS_{ij} - \sum_{i \in c: i>j} IS_{ji} \tag{2}$$

Where, IS_{ij} represents then number of selected data, $i \& j$ is an ordered pair of participant, WI_{v+1}^{i} computed weights with masks and $\sum_{i \in c: i<j}$ it can be denotes the remove of the duplicate data. To variation of the frequency is given in equation (3),

$$I_{v+1} = \frac{WI_{v+1}^{sum}}{|c|} \tag{3}$$

Where, $|c|$ denotes number of selected participants at time t , WI_{v+1}^{sum} is the initialized the relevant information. Finally, FNCF it improve image brightness, remove salt pepper noise, crop outer ring to have only ice particles in image. Then pre-processed data is fed to image segmentation phase.

C. Image Segmentation using Gaussian Mixture Model

In this section, Image Segmentation utilizing GMM is discussed [28].GMM is used for segmenting high-resolution scans. CT scan data is made up of several 2D images that are horizontal slices of core; all 2-D image is considered independently. To get ICMCT, a variety of kinds, resolves, modalities, ice features are accessible. Thus, along top 120 m of the ice core, CT images of porous material (such an ice-air mixture) with different densities are created, starting by lower-density snow (0.08 g/cm3), middle-density firn (0.35 g/cm3),higher-density polar ice (0.91 g/cm3). When a GMM is fitted to a pixel distribution, each class's Gaussian probability distribution is created, each with a weight provided to maintain the probability among zero, one. The components of the Gaussian mixture frequently correlate to distinct "types." It is assumed that there are two components in this instance: air and snow. Assuming that observed data is produced by combination of multiple Gaussian distributions, GMM is probabilistic method. Fundamental formula for a GMM's likelihood function is given in equation (4)

$$K(a \mid \xi) = \sum_{h=1}^{H} \kappa_h \Psi\left(a \mid \lambda_a, \Sigma_h\right) \tag{4}$$

Where ξ denotes vector of parameters distribution of observations related by cluster h , comprising variance, mean; λ_a denotes mixing coefficient of h^{th} distributions; λ_a denotes h^{th} component's mean; and $\sum_h$

signifies covariance matrix of the h^{th} component. In this example, a represents the observed data. Since dual clusters in this paper ice, air, observations are scalar intensity values, $\sum_h$ denotes 1 × 1 matrix.

The expectation-maximization (EM) algorithm's fundamental equations for expectation step, maximisation step, which are used to estimate a GMM's parameters, as below. E-Step: Using the initial step as a starting point, it determines expectation of component C_h for all data point in a. It is explained in equation (5)

$$\beta_{ph} = \frac{\kappa_h \Psi\left(a \mid \lambda_a, \sum_h\right)}{\sum_{l=1}^{H} \kappa_l \Psi\left(a_p \mid \lambda_l, \sum_l\right)} \tag{5}$$

The M-step then makes the following improvements to the model using the computed expectation β_{ph} and it is equated in equation (6) as follows,

$$\kappa_h = \frac{1}{P} \sum_{p=1}^{P} \beta_{ph} \tag{6}$$

The mixing coefficient is expressed in equation (7) as follows,

$$\lambda_a = \frac{1}{\sum_{p=1}^{P} \beta_{ph}} \sum_{p=1}^{P} \beta_{ph} a_p \tag{7}$$

Where a_p is the observed data in time through which the images are segmented and covariance matrix is calculated in equation (8)

$$\sum_l = \frac{1}{\sum_{p=1}^{P} \beta_{ph}} \sum_{p=1}^{P} \beta_{ph} \left(a_p - \kappa_h\right)\left(a_p - \kappa_h\right)^T \tag{8}$$

Each components share similar general covariance matrix when covariance matrix type is set to "tied," and it segment the ice core CT images and fed to classification process.

D. Classification using Dual Stream Spectrum Deconvolution Neural Network

In this section, the classification using DSSDNN [30] is discussed. DSSDNN is used to classifying micro scale CT images as sintered snow, compacted firn and bubbly ice. The gaining of spectrum devices is attributed to fixed spectrum degradation method. Current spectrum deconvolution technologies are responsive to handcrafted models, physically chosen parameters, as shown in Equation (9).

$$L = \left[J_2 - J_2\right] u\left(\begin{bmatrix} J_1 \\ -J_2 \end{bmatrix} \tilde{K} + \begin{bmatrix} o_1^h \\ o_1^y \end{bmatrix}\right) + o_2 \tag{9}$$

Where $(\tilde{K})$ denotes input, (L) signifies corresponding output from last layer. And $(J_1, J_2, o_1^h, o_1^y, o_2)$ denote the matrix parameters, in which (o_1^h, o_1^y) denotes bias that corresponding to upper stream, lower stream and (u) is the hidden layer function. In equation (10) the DSSDNN model to provide the best performance to classify the images as follows.

$$t(k) = \max(0, k+g) - \max(0, -k+g) \tag{10}$$

Where, (g) trainable parameter to combine these two streams into one unified framework and $g = (o_1^h + o_1^y)$ forward propagation able to be transformed. Partial derivative of $\left(t(k)\right)$ with respect to (g). The function corresponds to the last layer and it can be written as in equation (11),

$$L = J_2 t\left(J_1 K + \frac{o_1^h - o_1^y}{2}\right) + o_2 \tag{11}$$

Where, the function is defined as $(t), (o)$ denotes parameter, (L) signifies corresponding output from the last layer, these parameters guide forward propagation, which is learned using the back-propagation algorithm.

$(o_1^h - o_1^y)$ is the forward propagation. Let us consider $y_j = Y(l_j, s(k_j, \omega))$ where (y) the loss functions and (Y) is the objective function is function is given in equation (12).

$$Y(l_j, s(k_j, \omega)) = \frac{1}{2A}\sum_{j=1}(l_j - s(k_j, \omega))^2 \tag{12}$$

Where, network $s(k_j, \omega), (\omega)$ contains all parameters within the network, (k_j, l_j) denotes the degraded j^{-th} spectrum. (A) denotes number of training samples. Loss function is used mean-Square error (MSE). In equation (13), the parameter serves an initial value determining the learning pace as follows,

$$R(\omega, j:\eta) = \arg\min \sum_{j=1}^{a} i_j y_j - \eta i_j \tag{13}$$

Where (η) denotes parameter (R) is the number of true positive samples detected as CT image cases, (a) and (j) are the specificity and the sensitivity values, respectively, Finally, DSSDNN classifying micro scale CT images as sintered snow, compacted firn and bubbly ice. The AI-depend optimization technique is considered by DSSDNN classifier owing to its practicality, efficiency. The WSOA is allocated to enhance DSSDNN. Here, WSOA is allocated for turning weight ω, η parameter of DSSDNN.

E. Optimisation utilizing Water Strider Optimization Algorithm (WSOA)

The weights parameter ω, η of DSSDNN is enhanced using proposed WSOA [31].Initially, WSOA creates the uniformly dispersed populace for optimizing the initialization parameters of DSSDNN parameters. The Hemiptera order comprises the class of insects known as water striders, or Gerridae. Water striders likely existed on Earth for at than 50 million years, according to fossil records. They weigh ten dyeness and are around one centimetre long. Generally speaking, men have smaller bodies than women.

1) Stepwise process of WSOA

Here, stepwise process is defined to get ideal value of DSSDNN based on WSOA. Initially, WSOA makes the equally distributing populace to optimize the optimum parameter ω, η of DSSDNN. The ideal solution is promoted utilizing WSOA and the related flowchart is given in Figure 2.

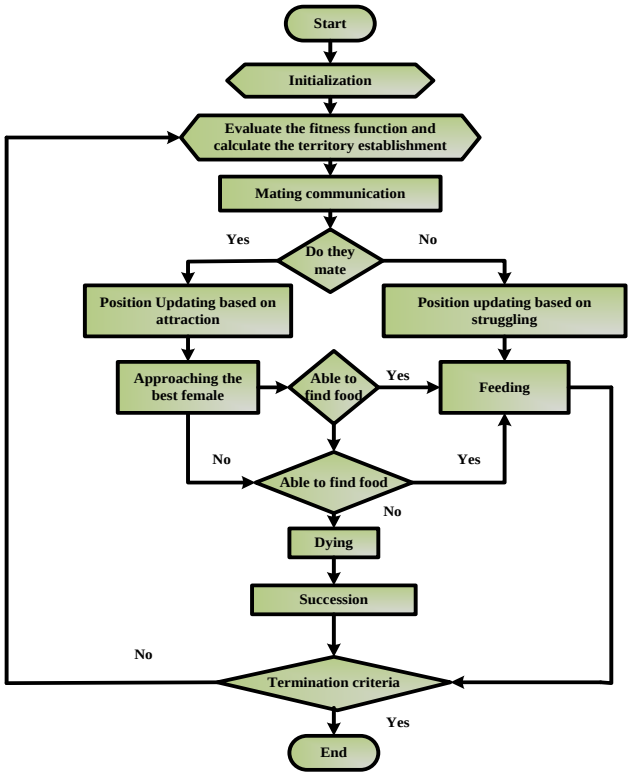

Figure 2: Flow chart of WSOA for optimizing DSSDNN parameters

Step 1: Initialization

Initialize input parameter, here input parameter are the gain parameters of DSSDNN which was denoted as $L, t(k)$.

$$A = \begin{bmatrix} a_{1,1} & a_{1,2} & \ldots & a_{1,d-1} & a_{1,d} \\ a_{2,1} & a_{2,2} & \ldots & a_{2,d-11} & a_{1,d} \\ : & : & a_{u,v} & : & : \\ a_{m,1} & a_{m,2} & \ldots & a_{m,d-1} & a_{m,d} \end{bmatrix} \tag{14}$$

Where, $a_{u,v}$ and m represent the number of water strider in a mound indicates where the v^{th} dimension of the u^{th} population.

Step 2: Random generation

After generalization,WSOA generates mechanism of moving towards the Water Strider Algorithm using input parameters chosen at random.

Step 3: Fitness function

The initialized parameters is depend on current best position are resolute. Compute fitness value for each individual,

$$fitness\ \ function = F = Optimizing[\omega, \eta] \tag{15}$$

Step 4: Exploration Phase

The five primary stages of the WSO algorithm birth, territory establishing, mating, eating, death are mathematically modelled. Throughout process, a lake is used to define search-space comprising various domains of solutions, and food represents the objective function metaphorically. The optimization problems were treated as maximization problems in the ensuing steps. Therefore, the solution is more optimal the higher the objective value. The water striders hatch from eggs that are dispersed across the lake. The random distribution is given in equation (16).

$$WS_i^0 = Ub + rand(Ub - Lb) \tag{16}$$

Where, WS_i^0 denoteslocation of the water strider, Ub and Lb denotes upper bound and lower bound relative to maximum and minimum allowable values, $rand$ denotes random nuber among 0, 1 and $i = 1,2,.....,nws$, where nws denotes the number of water striders (WSs). Water striders have an amazing mechanism during their mating season.They will approach and mate if female gives off attraction signal. After mating, novel position adjusted to spot among them while taking into account a circle wave. if the woman declines, the man will mount her; after that, the woman will dismount him and lead him away. The keystone will either mate or repel one another; in any case, its new location will be determined by equation (17).

$$\begin{cases} WS_i^{t+1} = WS_i^t + R * rand & if\ mating\ happens \\ WS_i^{t+1} = WS_i^t + R * (1 + rand) & otherwise \end{cases} \tag{17}$$

Where, WS_i^t denoteslocation of $i-th$ water strider in $t-th$ cycle, $rand$ denotes random number among 0, 1, R denoes the vector which initial point is position of male and end point is position of female in similar territory. The radius of the ripple wave is given in equation (18).

$$R = WS_F^{t-1} - WS_i^{t-1} \tag{18}$$

Where, WS_F^{t-1} represent the position of female water strider, WS_i^{t-1} is the position of male water strider in same territory. The Euclidean distance among male, female WSs is equal to the length of R.

Step 5: Exploitation Phase for optimizing ω, η

The process of mating needs a lot of energy, whether it is successful or not. Consequently, WSs in their new posture forage for food sources. The novel position around best water strider of the lake comprising deal of good food resources is given in equation (19).

$$WS_i^{t+1} = WS_i^t + 2 * rand * (WS_{BL}^t - WS_i^t) \tag{19}$$

Where, WS_{BL}^t denotes best water strider in lake, WS_i^t denotes position of $i-th$ water strider in $t-th$ cycle, $rand$ denotes random number among 0, 1. Novel matured larva take place of deceased WS as the keystone, location inside area is initialized at random as given in equation (20).

$$WS_i^{t+1} = Lb_j^t + 2 * rand * (Ub_j^t - Lb_j^t) \quad (20)$$

Where, Ub_j^t *and* Lb_j^t denotes maximum and minimum values of WS's location inside $j-th$ territory. The water strider (WS) will perish if its new fitness is lower since it will not only be unable to locate food, but also face a higher risk of conflict with other WSs in the destination territory.

Step 6: Termination Condition

In this stage, the weight parameter ω, η Dual Stream Spectrum Deconvolution Neural Network are optimized by support of WSOA, iteratively repeat step 3 until halting $t = t + 1$ is met**.** Then proposed ICMCTS-WSOA-DSSDNN-GMMpredicts the Ice-Core Micro-CT Image Segmentation with greater accuracy by lessening computational time, error rate.

IV. RESULT WITH DISCUSSION

Experimental results of suggested method are discussed. The suggested method is then simulated in python using the mentioned performance indicators. The proposed ICMCTS-WSOA-DSSDNN-GMMmethod is executed in python. Obtained outcome ofICMCTS-WSOA-DSSDNN-GMMmethod is analyzed with existing systems like ICMCTS-U-net-GMM, ICMCTS-KNN-GMM, ICMCTS-FCN-GMM.

A. Performance measures

It is a crucial step for selecting optimal classifier. Performance measures are assessed to assess performance, likes accuracy, recall, precision, F1-Score and ROC. To scale performance metrics, performance metric is deemed. To scale the performance metric, the True Negative, True Positive, False Negative, False Positive samples are needed.

- TN: number of pixels are wrongly labelled as target class.
- TP: number of pixels are accurately labelled as target class.
- FP: amount of pixels are wrongly identified as target class,
- FN: quantity of pixels ought to be classified as target class

1) Accuracy

It is a measurement of percentage of pixels in predicted segmentation that match ground truth segmentation in terms of proper classification and it is given in equation (21).

$$Accuracy = \frac{TP + TN}{TP + TN + FP + FN} \quad (21)$$

2) Precision

It is one indicator of ML method's performance the quality ofpositive prediction made by method. It refers to number of true positives divided by total positive predictions as given in equation (22).

$$\Pr ecision = \frac{TP}{TP + FP} \quad (22)$$

3) Recall

It known as true positive rate, is percentage of data samples that ML method correctly detects as belonging to class of interest. It is calculated using equation (23).

$$\mathrm{Re}\, call = \frac{TP}{TP + FN} \quad (23)$$

4) Jaccard Index (IoU)

It is measurement of overlap among anticipated, ground truth segmentations, and also referred to as Jaccard index. Definition of it is the ratio of the two segments' union to their intersection as given in equation (24).

$$IoU = \frac{TP}{TP + FP + FN} \quad (24)$$

5) ROC

It is ratio of false negative to the true positive area and it is given in equation (25)

$$ROC = 0.5 \times \left(\frac{TP}{TP + FN} + \frac{TN}{TN + FP} \right) \quad (25)$$

B. Performance analysis

Fig 3 to 9 portrays simulation outcomes of ICMCTS-WSOA-DSSDNN-GMMmethod. Then, the proposed ICMCTS-WSOA-DSSDNN-GMMmethod is analyzed with existing ICMCTS-U-net-GMM, ICMCTS-KNN-GMM and ICMCTS-FCN-GMM methods respectively.

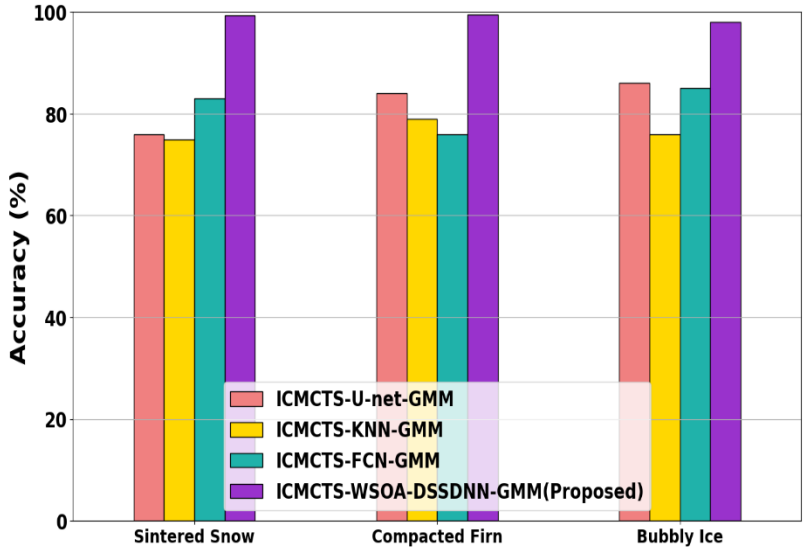

Figure: 3 Accuracy analysis

Figure 3 shows accuracy analysis. Here, ICMCTS-WSOA-DSSDNN-GMM method attains 21.51%, 52.38%, and 21.51% higher accuracy for sintered snow; 46.26%, 24.05%, 19.51% higher accuracy for compacted firn; 33.78%, 39.43%, 52.30% greater accuracy for bubbly ice; analysed with existing techniques such as ICMCTS-U-net-GMM, ICMCTS-KNN-GMM and ICMCTS-FCN-GMM respectively.

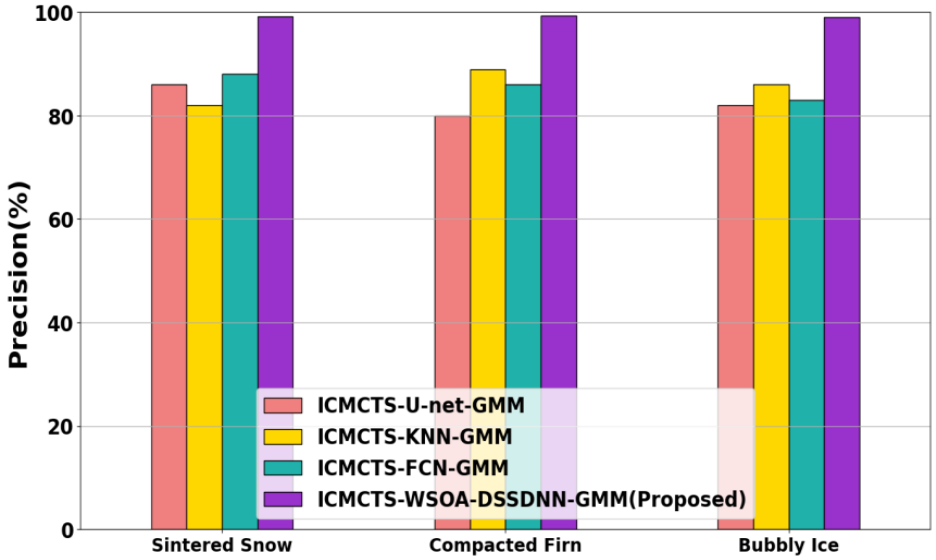

Figure 4: Precision analysis

Figure 4 shows precision analysis. Here, ICMCTS-WSOA-DSSDNN-GMM method attains28%, 50%, and 21.51% higher Precision for sintered snow; 41.79%, 20.25%, 15.85% higher Precision for compacted firn; 37.5%, 32%, 32% higher Precision for bubbly ice; analysed with existing techniques likes ICMCTS-U-net-GMM, ICMCTS-KNN-GMM and ICMCTS-FCN-GMM respectively.

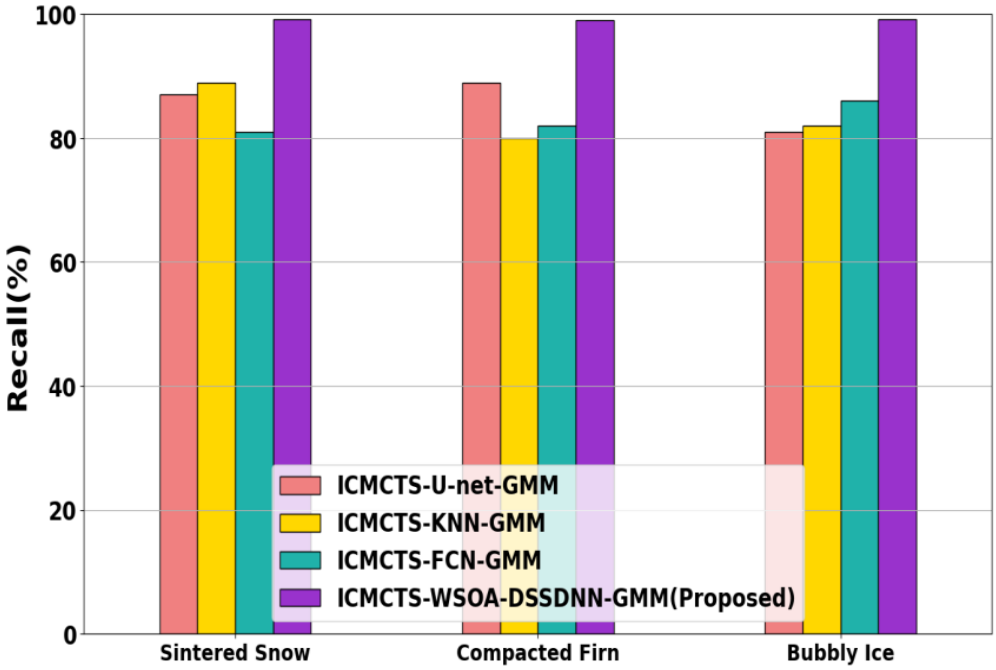

Figure 5: Recall analysis

Figure 5 shows recall analysis. Here, ICMCTS-WSOA-DSSDNN-GMM method attains23.07%, 41.17%, and 24.67% higher recall for sintered snow; 43.47%, 25.31%, 16.47% higher recall for compacted firn; 38.02%, 30.66%, 50.76% higher recall for bubbly ice analysed with existing techniques likes ICMCTS-U-net-GMM, ICMCTS-KNN-GMM and ICMCTS-FCN-GMM respectively.

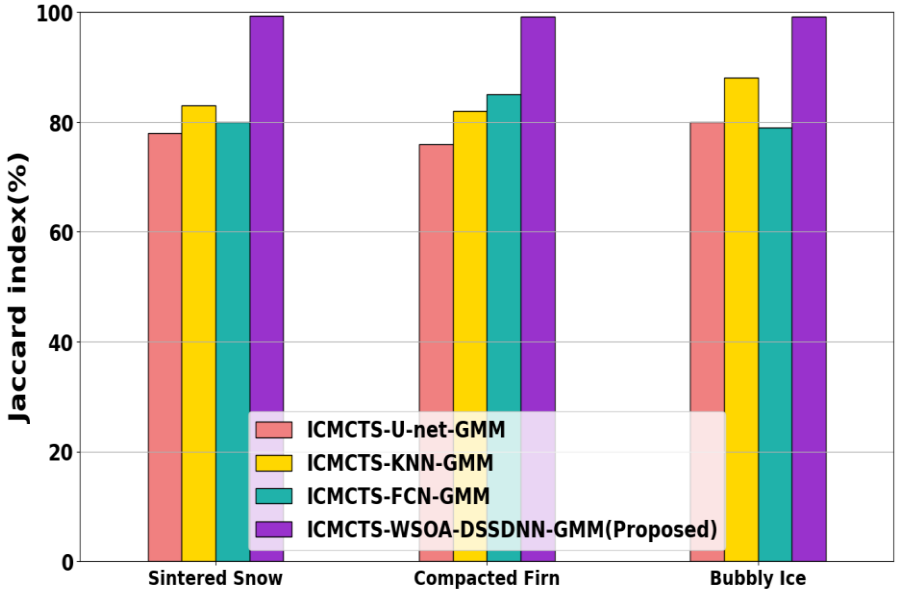

Figure 6: Jaccard Index (IoU) analysis

Figure 6 shows Jaccard Index (IoU) analysis. Here, ICMCTS-WSOA-DSSDNN-GMM method attains39.43%, 28.57%, and 33.78% higher Jaccard Index (IoU) for sintered snow; 44.77%, 40.57%, 49.23% higher Jaccard Index (IoU) for compacted firn; 57.37%, 31.50%, 35.21% higher Jaccard Index (IoU) for bubbly ice; analysed with existing techniques likes ICMCTS-U-net-GMM, ICMCTS-KNN-GMM and ICMCTS-FCN-GMM respectively.

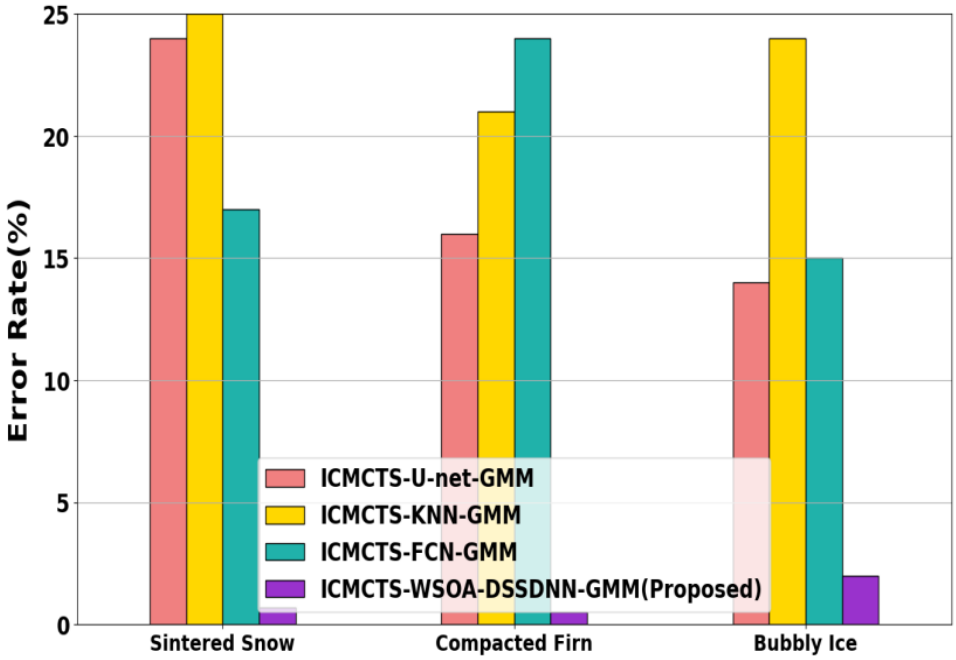

Figure 7: Error rate analysis

Figure 7 shows error rate analysis. Here, ICMCTS-WSOA-DSSDNN-GMM method attains15.85%, 23.37%, and 23.37% higher Error rate for sintered snow; 25.97%, 40.57%, 49.23% higher Error rate for compacted firn; 57.37%, 33.33%, 21.51% higher Error rate for bubbly ice analysed with existing techniques likes ICMCTS-U-net-GMM, ICMCTS-KNN-GMM and ICMCTS-FCN-GMM.

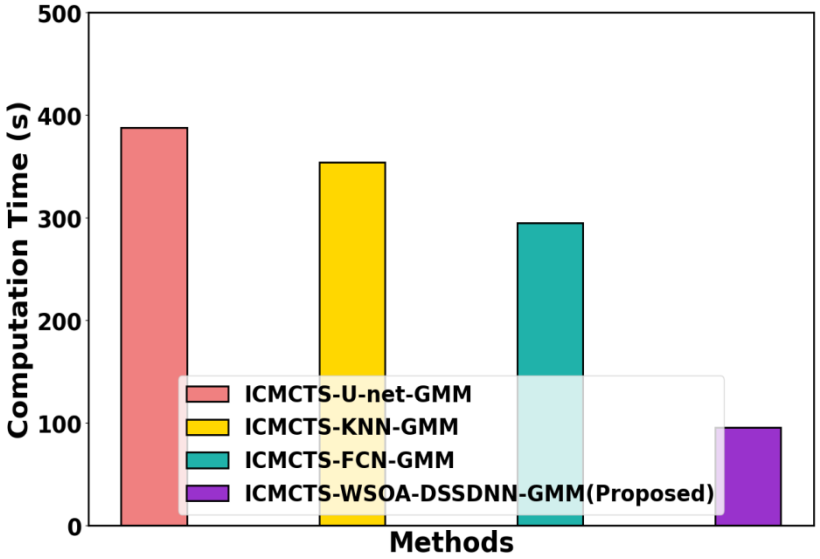

Figure 8: Computation time analysis

Figure 8 displays computation time analysis. Here, ICMCTS-WSOA-DSSDNN-GMMattains 28.8%, 25.4% and 23.5% lesser computation time analyzed with existing method likes ICMCTS-U-net-GMM, ICMCTS-KNN-GMM and ICMCTS-FCN-GMM models respectively.

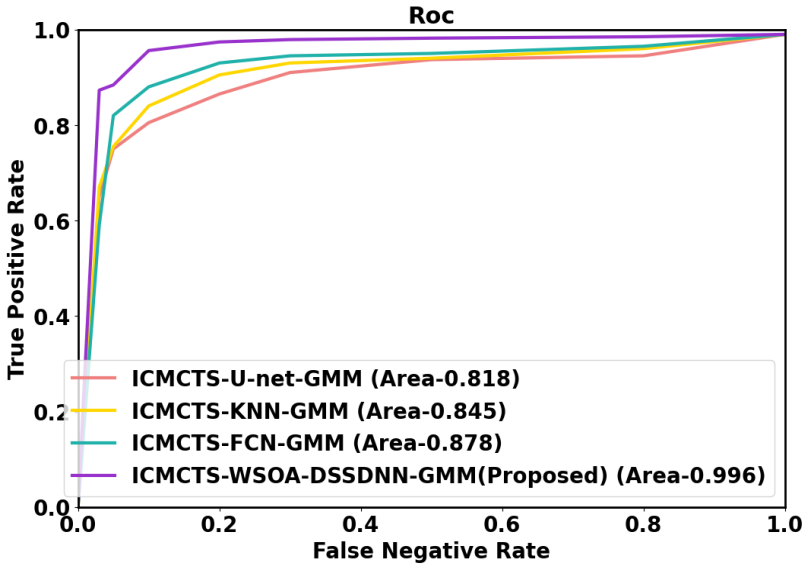

Figure 9: ROC analysis

Figure 9 depicts ROC analysis. Here, ICMCTS-WSOA-DSSDNN-GMM method attains 13.98%, 15.22%, 11.54% greater AUC analysed with existing methods like ICMCTS-U-net-GMM, ICMCTS-KNN-GMM and ICMCTS-FCN-GMM respectively

C. Discussion

A ICMCTS-WSOA-DSSDNN-GMMmodel for classifying micro scale CT images as sintered snow, compacted firn, bubbly ice is developed in this paper**.** Because DL method depends on generated ground truth, it is susceptible to errors of all kinds from a weak learner. The last core ground truth in this investigation had a number of problems, which decreased the DSSDNN ultimate accuracy in identifying some bubbles. Additionally, as the DSSDNN is susceptible to image misalignment, we must confirm that lower-resolution input image has precise equivalent down sampled higher-resolution ground truth before sending it to the DSSDNN. This stops the present strategy from achieving additional resolution discrepancies.

V. CONCLUSION

In this section, ICMCTS with Dual Stream Spectrum Deconvolution Neural Network and Gaussian Mixture Model (ICMCTS-WSOA-DSSDNN-GMM)is successfully implemented. The proposed ICMCTS-WSOA-DSSDNN-GMMmethod is executed in python. The performance of ICMCTS-WSOA-DSSDNN-GMM approach contains 16.24%, 17.90% and 27.7% high accuracy, 14.04%, 25.51% and 19.31% higher precision and 14.36%, 12.65% and 14.51% higher recall when analyzed to the existing methods like ICMCTS-U-net-GMM, ICMCTS-KNN-GMMand ICMCTS-FCN-GMMmethods respectively.

REFERENCE

[1] Karanam, S.R., Srinivas, Y., & Chakravarty, S. (2023). A statistical model approach based on the Gaussian Mixture Model for the diagnosis and classification of bone fractures. *International Journal of Healthcare Management*, 1-12.

[2] Ranjbarzadeh, R., Dorosti, S., Ghoushchi, S.J., Caputo, A., Tirkolaee, E.B., Ali, S.S., Arshadi, Z., & Bendechache, M. (2023). Breast tumor localization and segmentation using machine learning techniques: Overview of datasets, findings, and methods. *Computers in Biology and Medicine*, *152*, 106443.

[3] Chen, M., Toader, B., & Lederman, R., (2023). Integrating molecular models into CryoEM heterogeneity analysis using scalable high-resolution deep Gaussian mixture models. *Journal of Molecular Biology*, *435*(9), 168014.

[4] Kang, H., Witanto, J.N., Pratama, K., Lee, D., Choi, K.S., Choi, S.H., Kim, K.M., Kim, M.S., Kim, J.W., Kim, Y.H., & Park, S.J. (2023). Fully Automated MRI Segmentation and Volumetric Measurement of Intracranial Meningioma Using Deep Learning. *Journal of Magnetic Resonance Imaging*, *57*(3), 871-881.

[5] Oluwasegun, A., & Jung, J.C. (2023). A multivariate Gaussian mixture model for anomaly detection in transient current signature of control element drive mechanism. *Nuclear Engineering and Design*, *402*, 112098.

[6] Tung, P.Y., Sheikh, H.A., Ball, M., Nabiei, F., & Harrison, R.J. (2023). SIGMA: Spectral interpretation using gaussian mixtures and autoencoder. *Geochemistry, Geophysics, Geosystems*, *24*(1), e2022GC010530.

[7] Algumaei, A., Azam, M., Najar, F., & Bouguila, N. (2023). Bounded multivariate generalized Gaussian mixture model using ICA and IVA. *Pattern Analysis and Applications*, 1-30.

[8] Balamurugan, T., & Gnanamanoharan, E. (2023). Brain tumor segmentation and classification using hybrid deep CNN with LuNetClassifier. *Neural Computing and Applications*, *35*(6), 4739-4753.

[9] Xu, K., Jin, Q., Li, J., Ushizima, D.M., Li, V.C., Kurtis, K.E., & Monteiro, P.J. (2023). In-situ microtomography image segmentation for characterizing strain-hardening cementitious composites under tension using machine learning. *Cement and Concrete Research*, *169*, 107164.

[10] Saranya, P., Pranati, R., & Patro, S.S. (2023). Detection and classification of red lesions from retinal images for diabetic retinopathy detection using deep learning models. *Multimedia Tools and Applications*, 1-21.

[11] Lee, S.Y., Le, T.H.M., & Kim, Y.M. (2023). Prediction and detection of potholes in urban roads: Machine learning and deep learning based image segmentation approaches. *Developments in the Built Environment*, *13*, 100109.

[12] Niknam, G., Molaei, S., Zare, H., Clifton, D., & Pan, S. (2023). Graph representation learning based on deep generative gaussian mixture models. *Neurocomputing*, *523*, 157-169.

[13] Iwata, T. (2023). Meta-learning representations for clustering with infinite gaussian mixture models. *Neurocomputing*, 126423.

[14] Naik, D.A., Mohana, R.M., Ramu, G., Lalitha, Y.S., SureshKumar, M., & Raghavender, K.V. (2023). Analyzing histopathological images by using machine learning techniques. *Applied Nanoscience*, *13*(3), 2507-2513.

[15] Chen, X., Xue, Y., Zhu, Y., & Ma, R. (2023). A novel smoke detection algorithm based on improved mixed Gaussian and YOLOv5 for textile workshop environments. *IET Image Processing*, *17*(7), 1991-2004.

[16] Jin, M., Sun, C., & Hu, Y. (2023). An intelligent traffic detection approach for vehicles on highway using pattern recognition and deep learning. *Soft Computing*, *27*(8), 5041-5052.

[17] Liu, L., Zhang, P., Liang, G., Xiong, S., Wang, J., & Zheng, G. (2023). A spatiotemporal correlation deep learning network for brain penumbra disease. *Neurocomputing*, *520*, 274-283.

[18] Aziz, R.M., Desai, N.P., & Baluch, M.F. (2023). Computer vision model with novel cuckoo search based deep learning approach for classification of fish image. *Multimedia Tools and Applications*, *82*(3), 3677-3696.

[19] Singh, H., Ahmed, A.S., Melandsø, F., & Habib, A. (2023). Ultrasonic image denoising using machine learning in point contact excitation and detection method. *Ultrasonics*, *127*, 106834.

[20] Allada, A., Bhavani, R., Chaduvula, K., & Priya, R. (2023). Early Diagnosis of Alzheimer Disease from Mri Using Deep Learning Models. *Journal of Information Technology Management*, *15*(Special Issue), 52-71.

[21] Külah, E., Çetinkaya, Y.M., Özer, A.G. & Alemdar, H. (2023). COVID-19 forecasting using shifted Gaussian Mixture Model with similarity-based estimation. *Expert Systems with Applications*, *214*, 119034.

[22] Bagherzadeh, F., Freitag, J., Frese, U., & Wilhelms, F. (2023). Ice-Core Micro-CT Image Segmentation With Deep Learning and Gaussian Mixture Model. *IEEE Transactions on Geoscience and Remote Sensing*, *61*, 1-11.

[23] Saygılı, A. (2022). Computer-aided detection of COVID-19 from CT images based on Gaussian mixture model and kernel support vector machines classifier. *Arabian Journal for Science and Engineering*, *47*(2), 2435-2453.

[24] Liang, C., Wang, W., Miao, J., & Yang, Y. (2022). Gmmseg: Gaussian mixture based generative semantic segmentation models. *Advances in Neural Information Processing Systems*, *35*, 31360-31375.

[25] Wang, J., Gao, J., Yuan, Y., & Wang, Q. (2023). Crowd localization from gaussian mixture scoped knowledge and scoped teacher. *IEEE Transactions on Image Processing*, *32*, 1802-1814.

[26] Goel, K., Michael, N., & Tabib, W. (2023). Probabilistic Point Cloud Modeling via Self-Organizing Gaussian Mixture Models. *IEEE Robotics and Automation Letters*, *8*(5), 2526-2533.

[27] Ajay, P., Nagaraj, B., Kumar, R.A., Huang, R., & Ananthi, P. (2022). Unsupervised hyperspectral microscopic image segmentation using deep embedded clustering algorithm. *Scanning*, *2022*.

[28] Xiong, Y., Liang, L., Wang, L., She, J., & Wu, M. (2020). Identification of cash crop diseases using automatic image segmentation algorithm and deep learning with expanded dataset. *Computers and Electronics in Agriculture*, *177*, 105712.

[29] Perifanis, V., & Efraimidis, P.S. (2022). Federated neural collaborative filtering. *Knowledge-Based Systems*, *242*, 108441.

[30] Deng, L., Xu, G., Dai, Y., & Zhu, H. (2021). A dual stream spectrum deconvolution neural network. *IEEE Transactions on Industrial Informatics*, *18*(5), 3086-3094.

[31] Kaveh, A., Malek, N.G., Eslamlou, A.D., & Azimi, M. (2023). An open-source framework for the FE modeling and optimal design of fiber-steered variable-stiffness composite cylinders using water strider algorithm. *Mechanics Based Design of Structures and Machines*, *51*(1), 138-158.